Intrinsic and magnetic-field-induced linear polarization of excitons in ultrathin indirect-gap type-II GaAs/AlAs quantum wells

T. S. Shamirzaev,[1,2] J. Rautert,[3] D. R. Yakovlev,[3,4] M. M. Glazov,[4,5] and M. Bayer[3,4]

[1]*Rzhanov Institute of Semiconductor Physics, Siberian Branch of the Russian Academy of Sciences, 630090 Novosibirsk, Russia*

[2]*Ural Federal University, 620002 Yekaterinburg, Russia*

[3]*Experimentelle Physik 2, Technische Universität Dortmund, 44227 Dortmund, Germany*

[4]*Ioffe Institute, Russian Academy of Sciences, 194021 St. Petersburg, Russia*

[5]*Spin Optics Laboratory, Saint Petersburg State University, 198504 Peterhof, St. Petersburg, Russia*

(Received 10 February 2019; revised manuscript received 21 March 2019; published 5 April 2019)

The exciton dynamics in transverse magnetic field is investigated both experimentally and theoretically in two-monolayer-thick GaAs/AlAs quantum wells with an indirect band gap and a type-II band alignment. The observed linear polarization of the quantum well photoluminescence has two contributions, one of which arises from the crystalline structure of the quantum well. It does not depend on temperature and demonstrates a strong spectral dependence across the emission band. The other one is induced by a transverse magnetic field. It strongly decreases with increasing temperature, has no spectral dependence, and demonstrates an unexpectedly long-time dynamics. The experimental findings can be explained in the framework of the developed theoretical model which accounts for the quantum well anisotropy, the Zeeman effect of electrons and holes in the transverse magnetic field, and the redistribution of excitons over the spin sublevels. It provides quantitative agreement with the experiment and allows us to evaluate, for the studied structure, the heavy-hole in-plane g-factor tensor, which turns out to be extremely anisotropic with principal values of opposite signs and the same magnitude of 0.25.

DOI: 10.1103/PhysRevB.99.155301

I. INTRODUCTION

Electron-hole pairs or excitons determine the optical properties of semiconductors [1,2]. Excitons in semiconductors approaching the limit of two-dimensional behavior like in monolayer crystals [3], stacking faults in III-V and II-VI semiconductors [4,5], and quantum wells (QWs) of monolayer thickness [6,7] attract increased attention nowadays due to their unusual fine structure of the energy level spectrum, nontrivial kinetics, and spin dynamics.

In this regard, type-II heterostructures with spatially separated electrons and holes are particularly promising due to the long lifetimes of excitons. A very special case is realized in indirect band-gap heterostructures with type-II band alignment which demonstrate exciton lifetimes up to milliseconds, owing to the combination of electron-hole separation both in energy and momentum space [6–9]. Therefore, in this type of structure one can study long-lived exciton spin dynamics without the usual limitations imposed by the radiative decay of the electron-hole pairs in QWs with type-I band alignment.

Recently, we demonstrated that the magnetic-field-induced circular polarization and the related spin dynamics of excitons in type-II GaAs/AlAs QWs are the result of the redistribution in exciton population between optically bright and dark states. The population can be controlled both by thermodynamical parameters, i.e., the ratio of the exciton Zeeman splitting and the thermal energy, and by kinetic parameters, i.e., the relation between the various relaxation and recombination times in the system, that depend also on temperature and magnetic field [6,7].

The circular polarization of the exciton emission studied in Ref. [7] is induced by a longitudinal component of the magnetic field, normal to the QW. It follows from symmetry arguments that the transverse magnetic field, by contrast, does not result in any circular polarization, but should give rise to a linear polarization of emitted light. However, this effect has not been studied so far in corresponding QWs.

In this paper, we investigate the effects of a transverse magnetic field on the exciton "alignment." Namely, we measure the degree of linear polarization in ultrathin GaAs/AlAs QWs with indirect band gap and type-II band alignment. Two contributions to the linear polarization degree (P_l) of the QW exciton photoluminescence (PL) are found: (i) one comes from the QW crystalline structure and (ii) the other is induced by the transverse magnetic field. Unexpectedly, P_l demonstrates a long-lasting temporal dynamics in magnetic field. To explain the experimental data, we extend the model developed in our previous work [6,7] by taking into account a small, but nonzero in-plane g factor of the heavy holes.

The paper is organized as follows. In Sec. II the studied sample and the used experimental techniques are described. In Sec. III we present the experimental data on the linear polarization of the time-integrated and time-resolved photoluminescence recorded in external magnetic field. The developed model is presented in Sec. IV. The experimental data are analyzed and discussed in Sec. V.

II. EXPERIMENTAL DETAILS

The ultrathin GaAs/AlAs QW structure was grown by molecular-beam epitaxy on a semi-insulating (001)-oriented

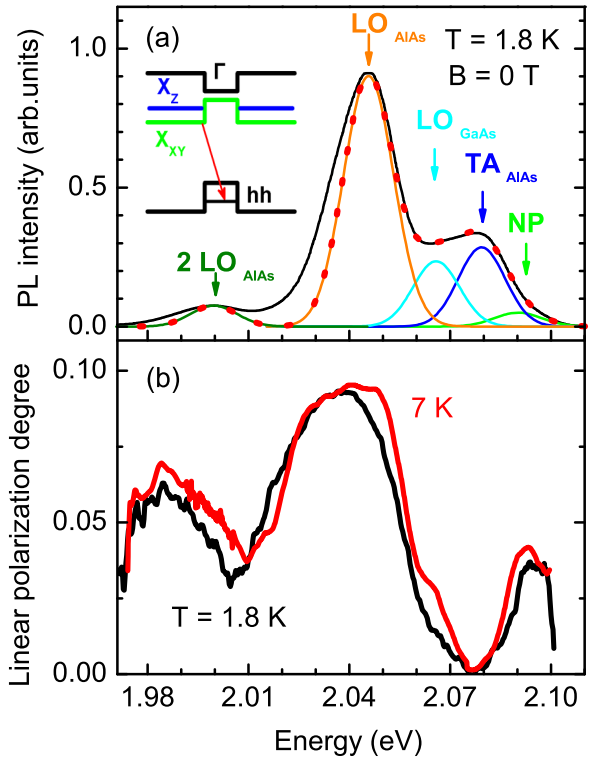

FIG. 1. (a) Time-integrated PL spectrum of the ultrathin GaAs/AlAs QW (black line) fitted with five Gaussian lines corresponding to the exciton recombination with and without involvement of phonons. The green, blue, cyan, orange, and olive solid lines are the no-phonon, TA_{AlAs}, LO_{GaAs}, LO_{AlAs}, and $2LO_{AlAs}$ phonon lines, respectively. The red dotted line is the fitted spectrum composed of the five lines. The inset shows the schematic band alignment of the structure with the QW in the middle. The red arrow marks the optical transition of the indirect exciton to the system ground state (see Ref. [6] for details). (b) Spectral dependence of the linear polarization degree of the exciton emission in the $x \parallel [1\bar{1}0]$ and $y \parallel [110]$ crystalline axes frame for temperatures of 1.8 and 7 K and at zero magnetic field.

GaAs substrate in a Riber Compact system. The sample consists of the GaAs QW layer embedded between 50-nm-thick layers of AlAs grown on top of a 200-nm-thick GaAs buffer layer [10]. The substrate temperature during the growth was 600 °C. The GaAs QW layer was deposited with a nominal thickness of two monolayers. A 20-nm-thick GaAs cap layer protects the top AlAs layer against oxidation. Further growth details are given in Ref. [9]. The GaAs/AlAs QW has a type-II band alignment with the lowest conduction-band states at the X_x and X_y minima of the AlAs conduction band and the heavy-hole (hh) states in the GaAs valence band [9,11,12]. A schematic band diagram of the structure and the optical transition of the indirect exciton to the system ground state are presented in the inset of Fig. 1(a).

The sample is placed in a split-coil magnet cryostat and exposed to magnetic fields up to $B = 10$ T. The temperature is varied from $T = 1.65$ up to 7 K. The photoluminescence is excited by the third harmonic of a Q-switched Nd : YVO_4 laser (3.49 eV) with a pulse duration of 5 ns. The pulse energy density is kept below 100 nJ/cm^2 and the pulse-repetition frequency is varied from 20 Hz up to 1 kHz [6]. The emitted light is dispersed by a 0.5-m monochromator. For time-integrated measurements the photoluminescence is detected by a liquid-nitrogen-cooled charge-coupled-device (CCD) camera. For time-resolved measurements a GaAs photomultiplier combined with a time-correlated photon-counting module is used. In order to monitor the PL decay in a wide temporal range of up to 1 ms, the time resolution of the detection system (i.e., the binning range of the photon-counting events) is varied between 100 ns and 10 μs.

The angle θ between the magnetic field direction and the QW growth axis ([001] direction that are denoted here as z axis) is selected to be equal to 90° (Voigt geometry). The crystallographic directions $[1\bar{1}0]$ and [110] in the QW plane are denoted as x and y axes, respectively. These are the main crystallographic axes of our studied structure, which has C_{2v} point symmetry. The emission is collected along the QW growth axis (z axis).

In order to determine direction and degree of the PL linear polarization the intensity of emission is studied as function of the orientation of a half-wave plate introduced in front of the analyzer (Glan-Taylor prism) which is mounted along the [001] direction of the QW. The angle $\varphi = 0°$ corresponds to the orientation of the half-wave plate axis along the magnetic field direction and rotation of half-wave plate axis on the angle of 45° corresponds to $\varphi = 90°$. For zero magnetic field measurements at $\varphi = 0°$ half-wave plate axis was oriented along the x axis. The sample is rotated around the z axis and the angle between the magnetic field direction and the $x \parallel [1\bar{1}0]$ axis in the QW plane is φ_B. The linear polarization degree P_l is evaluated from the data using the standard expression

$$P_l = \frac{I_x - I_y}{I_x + I_y},$$

where I_x and I_y are the intensities of the PL components along the x and y axes. As the excitation energy is well above the recombination energy, no effect of the excitation polarization on the PL polarization is found in our experiments.

III. EXPERIMENTAL RESULTS

A time-integrated photoluminescence spectrum of the ultrathin GaAs/AlAs QW is shown in Fig. 1(a) by the black line. The spectrum is composed of several lines corresponding to the contributions from several emission processes: It contains the no-phonon line (NP) and several lines of phonon-assisted recombination involving optical and acoustic phonons of GaAs and AlAs. The replicas associated with the transverse acoustic (TA) phonons of AlAs (phonon energy of 12 meV) as well as the longitudinal optical (LO) phonons of GaAs (30 meV) and AlAs (48 meV), all at the X point of the Brillouin zone [13], can be resolved. An additional feature can be assigned to the two AlAs LO-phonon assisted emission. The lines are broadened due to the roughness of the QW interfaces and fluctuations of the alloy composition and material amount [9,14]. An example of fitting the PL spectrum by five contributing Gaussian curves, each with the same full width at half-maximum of 19 meV, is shown in Fig. 1(a) by the red dotted line [6]. The deviation of the fitted spectrum from the experimental one in the low-energy region may result

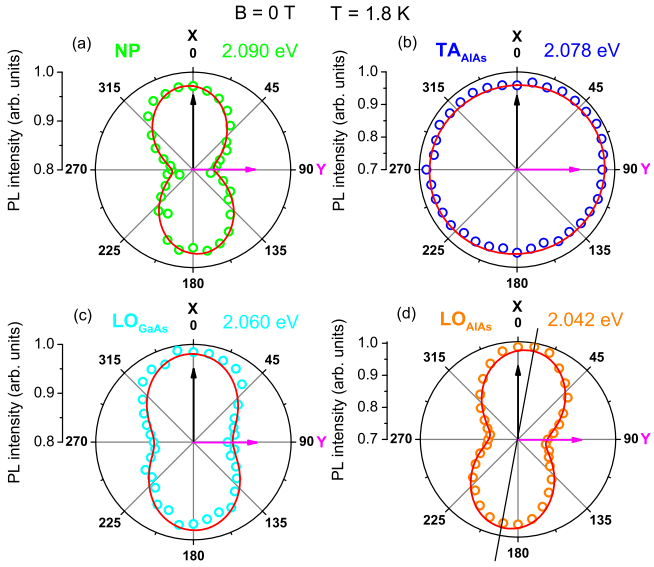

FIG. 2. Zero-field in-plane angular dependencies of the PL intensity selected by a linear polarization analyzer for (a) the NP transition, and its phonon replicas corresponding to the (b) TA_{AlAs}, (c) LO_{GaAs}, and (d) LO_{AlAs} phonons. $T = 1.8$ K. The axes choice is $x \parallel [1\bar{1}0]$ and $y \parallel [110]$. The angle $\varphi = 0^\circ$ corresponds to the orientation of the half-wave plate axis along x axis. The red solid lines show the fitting results with the parameters given in the text.

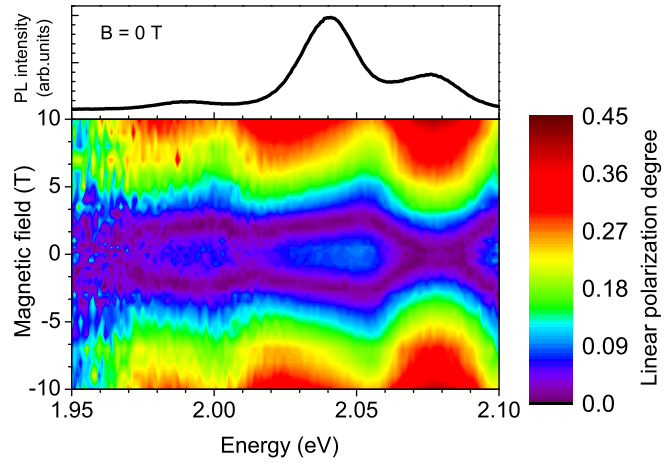

FIG. 3. Spectral dependence of the absolute value of the linear polarization degree P_l in the $x \parallel [1\bar{1}0]$ and $y \parallel [110]$ crystal axes frame as a function of magnetic field strength at temperature 1.8 K. The black line shows the PL spectrum of the QW.

from two-phonon transitions involving acoustic phonons that are not taken into account in the fitting procedure.

Even at zero magnetic field, the PL emission is linearly polarized. We call it an intrinsic linear polarization to distinguish from the polarization induced by external magnetic field. The intrinsic P_l has a strong spectral dependence across the emission band as is shown Fig. 1(b). The P_l measured in the frame of the (xy) axes equals to 3.5% for the NP line. It decreases down to 0 for the TA_{AlAs} phonon-assisted line and increases again up to 9.5% for the LO_{AlAs} phonon-assisted line. The polarization degree practically does not change with temperature in the range from 1.8 to 7 K.

The angular dependencies of the emission intensity, selected by a linear polarization analyzer, for the NP and its phonon-assisted recombination lines are presented in Fig. 2. One can see that the emission of the TA_{AlAs} phonon-assisted recombination line is not polarized and the polarization of the emission related to the NP [Fig. 2(a)] and LO_{GaAs} [Fig. 2(c)] lines is oriented along the x axis, while the polarization of the LO_{AlAs} [Fig. 2(d)] phonon-assisted recombination line is slightly rotated by an angle of 15° from the x axis, possibly due to structure imperfections [15].

The application of a transverse magnetic field strongly changes the linear polarization of the emission as shown by the absolute $|P_l|$ value in Fig. 3. In magnetic field, the spectral dependence of P_l across the emission band remains the same, while the polarization degree increases. Let us consider that in more detail for different emission lines.

We start with consideration of the TA_{AlAs} line which intrinsic linear polarization at zero magnetic field is absent. Magnetic-field-induced linear polarization appears with increasing magnetic field and is oriented along the y axis. The degree of linear polarization at a fixed field strength does not depend on the angle between the crystallographic direction $[1\bar{1}0]$ (x axis) and the direction of the magnetic field φ_B, as one can clearly see in Fig. 4, where φ_B is changed from 0° to 45° and then to 90°. One can also see in Figs. 5(a) and 5(c) that the main axes of P_l are linked to the crystallographic directions, with P_l maximum along the y axis, irrespective with the magnetic field strength and orientation as well as with sample temperature. Here, φ_L is an angle between the main axis of the linear polarization diagram having maximal PL intensity and x axis.

The absolute value of the magnetic-field-induced polarization degree of the TA_{AlAs} line increases monotonically with increasing field strength up to 40% for $B = 10$ T at $T = 1.65$ K [Fig. 5(e)]. The $|P_l|$ value at fixed magnetic field decreases with increasing temperature. For example, at $B = 10$ T an increase of temperature from 1.65 to 5 K results in a decrease of $|P_l|$ from 40% down to 13% [see Fig. 5(e)].

The polarization of the emission at the NP, LO_{GaAs}, and LO_{AlAs} lines is also modified by the magnetic field. These lines have a finite intrinsic P_l at zero magnetic field, which is oriented along the x axis. While the magnetic-field-induced P_l is oriented along the y axis, similar to what we have seen for the TA_{AlAs} line. The properties of P_l in magnetic field are controlled by the competition of the intrinsic and magnetic-field-induced contributions. All these PL lines show similar changes in the polarization degree and orientation with varying temperature, magnetic field strength, and sample orientation. Therefore, we present and discuss below the typical behavior of the LO_{AlAs} phonon-assisted line that is the strongest in intensity.

The in-plane angular dependencies of the LO_{AlAs} line intensity, selected by a linear polarizer and measured at $T = 1.8$ K for different magnetic fields oriented along the x axis, are shown in Fig. 6. In contract to the TA_{AlAs} line, the LO_{AlAs} emission has an intrinsic polarization along the x axis at zero magnetic field [Fig. 6(a)]. In strong field of 10 T, where the magnetic-field-induced contribution dominates, the P_l is

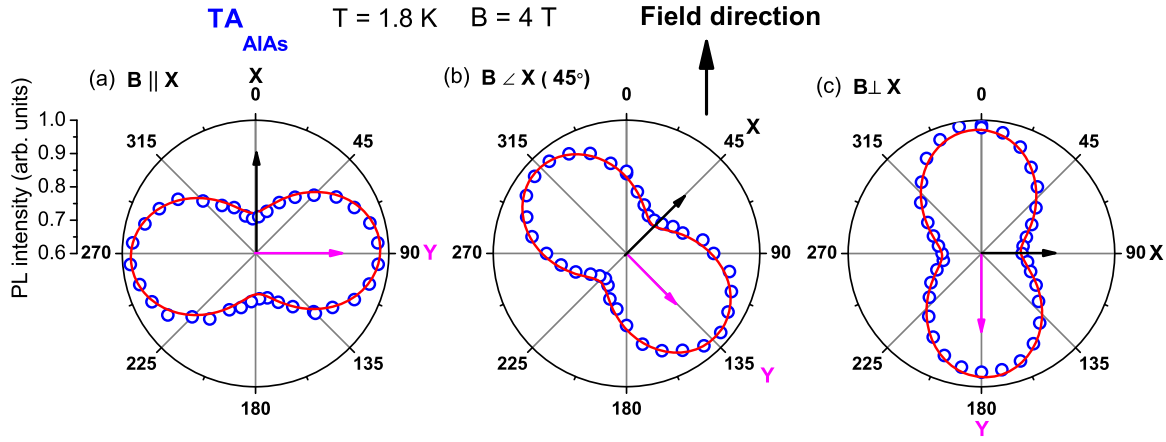

FIG. 4. In-plane angular dependencies of the emission intensity selected by a linear polarization analyzer for the emission of the TA_{AlAs} line measured at $T = 1.8$ K and $B = 4$ T for different angles between the magnetic field and the crystallographic direction $x \parallel [1\bar{1}0]$, φ_B: (a) 0°, (b) 45°, and (c) 90°. The axes assignments are $x \parallel [1\bar{1}0]$ and $y \parallel [110]$. The red solid lines show the results of fitting with the parameters given in the text.

aligned along the y axes [Fig. 6(e)]. In intermediate fields the P_l value shows nonmonotonic behavior with changing sign, which reflects the rotation of P_l from x axis to y axes [Fig. 5(f)]. The rotation of the polarization direction is clearly seen from $\varphi_L(B)$ dependence in Fig. 5(b). Note, that similar to the TA_{AlAs} line the polarization direction and degree of the LO_{AlAs} line are determined by magnetic field strength and do not depend on the field orientation angle φ_B.

The temperature increase weakens the magnetic-field-induced P_l, but has no effect on the intrinsic P_l. One can see that in Fig. 5(d), where φ_L, e.g., at $B = 8$ T changes from 90° back to 0° with temperature change form 1.8 up to 6.2 K. The polarization degree $P_l(B)$ also demonstrates diminishing of the magnetic-field-induced contribution for higher temperatures [Fig. 5(f)]. Note that temperature dependencies of $P_l(B)$ for LO_{AlAs} line just repeat the dependencies of TA_{AlAs} line with a constant offset, which is equal to the intrinsic polarization degree [compare Figs. 5(f) and 5(e)].

The information on the relative time scales of the spin and recombination dynamics is very important to understand redistribution dynamics of exciton population between bright and dark exciton states. The temporal dynamics of the LO_{AlAs} line intensity in a magnetic field of 6 T for the two linear polarized components I_x and I_y corresponding to the x and y main axes, respectively, and the dynamics of the linear polarization degree $P_l(t)$ for different magnetic field strengths are shown in Figs. 7(a) and 7(b), respectively.

In zero magnetic field the intrinsic polarization degree does not change with time, while the magnetic-field-induced contribution to P_l has dynamics with surprisingly long times up to 100 μs [Fig. 7(b)]. The absolute value of the polarization degree saturates at a value that depends on the magnetic

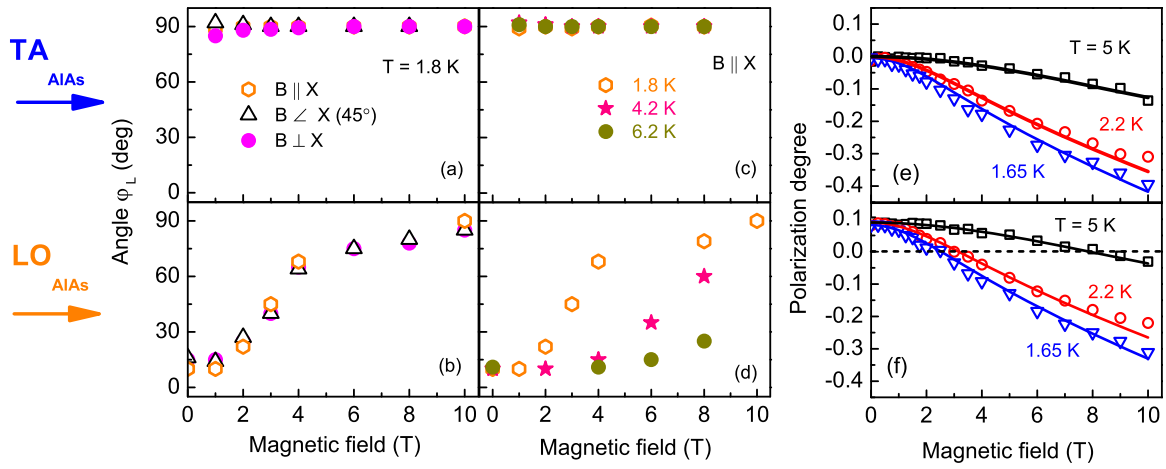

FIG. 5. Angle φ_L between direction of the linear polarization of the emission and x axis as a function of the magnetic field strength measured for different angles φ_B between the magnetic field and the crystallographic direction $[1\bar{1}0]$ (x axis) and temperatures. $\varphi_L = 0°$ and 90° correspond to the linear polarization directions along the x axis and y axis, respectively. (a), (b) $\varphi_B = 0°$, 45°, and 90° at $T = 1.8$ K, (c), (d) $\varphi_B = 0°$ at $T = 1.8$, 4.2, and 6 K for the TA_{AlAs} (a), (c) and LO_{AlAs} (b), (d) lines. Linear polarization degree P_l as a function of the magnetic field measured at $T = 1.65$, 2.2, and 5 K for (e) TA_{AlAs} line and (f) LO_{AlAs} line. The solid lines show the results of modeling with the parameters given in the text.

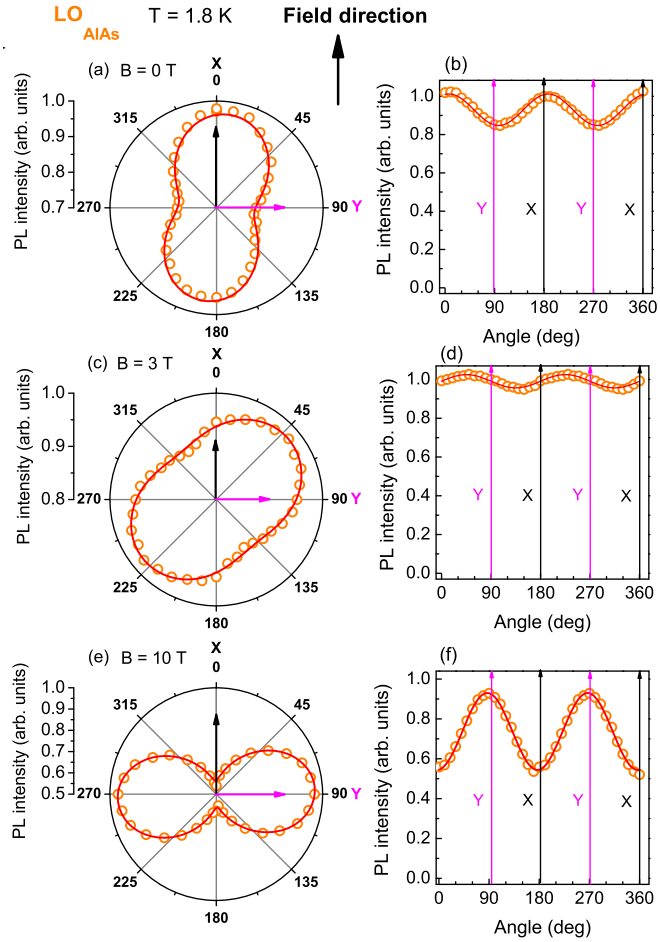

FIG. 6. In-plane angular dependencies of the PL intensity selected by a linear polarization analyzer for the emission at the LO_{AlAs} phonon line, namely, at 2.042 eV, measured for $T = 1.8$ K, at various magnetic field strengths: (a), (b) 0 T, (c), (d) 3 T, and (e), (f) 10 T. The magnetic field is oriented along the crystallographic direction $x \parallel [1\bar{1}0]$; the y axis is parallel to [110]. The red solid lines show the results of fitting with the parameters given in the text.

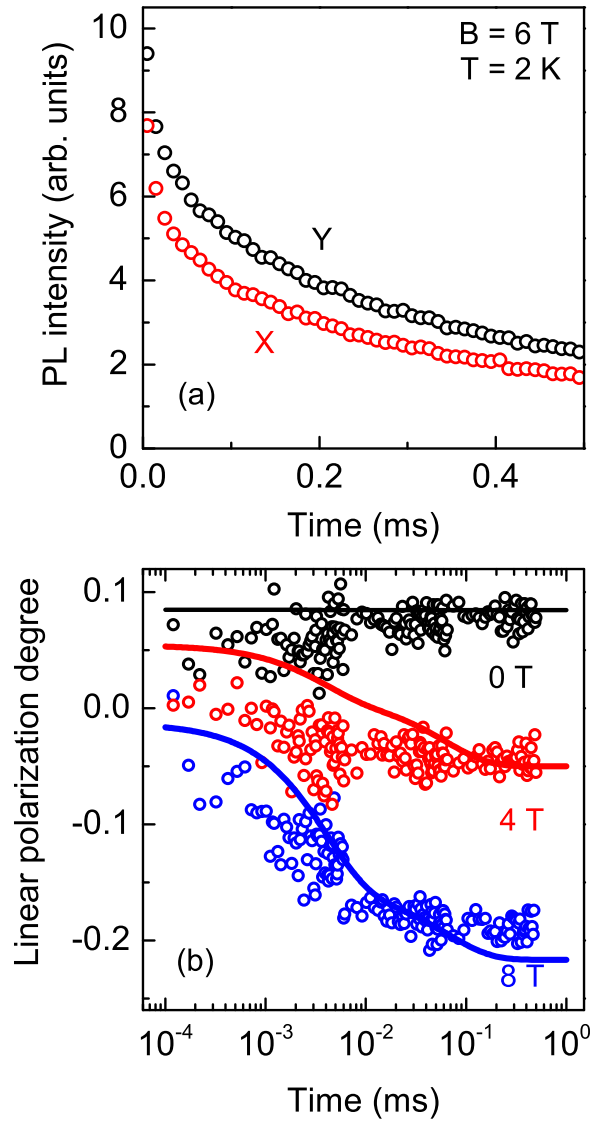

FIG. 7. (a) PL recombination dynamics of the LO_{AlAs} phonon line in a magnetic field 6 T for the two linear polarized components I_x and I_y directed along the $x \parallel [1\bar{1}0]$ and $y \parallel [110]$ axes, respectively. (b) Dynamics of the linear polarization degree $P_l(t)$ for different magnetic field strengths of 0, 4 and 8 T. $T = 2$ K. The solid lines show the results of fitting with the parameters given in the text.

field strength. This experiment clearly shows the different origins of the intrinsic and magnetic-field-induced contributions to P_l.

Let us summarize the most important experimental findings: (i) In zero magnetic field there is an intrinsic linear polarization of the emission that is nonmonotonic across the PL spectrum of the GaAs/AlAs QW. The absolute value of the linear polarization degree changes from zero for the TA_{AlAs} phonon-assisted line up to 9.5% for the LO_{AlAs} phonon-assisted line. (ii) Transverse magnetic field induces an additional contribution in linear polarization of the emission that is uniform across the PL spectrum. The orientation of the magnetic field in the QW plane does not affect the polarization of the emission. The linear polarization degree of emission is determined by the magnetic field strength and the temperature only. (iii) The linear polarization degree demonstrates an unusual long-lasting (in the microsecond range) dynamics in magnetic field; the P_l does not change with time at $B = 0$.

IV. THEORY

A. Symmetry analysis

Quantum wells grown from zinc-blende lattice semiconductors along the cubic axis $z \parallel [001]$ can possess the D_{2d} or the C_{2v} point symmetry group: the former is realized in heterostructures with symmetric potential, while the latter is typical for quantum wells with asymmetric potential, nonequivalent interfaces, or in presence of an in-plane anisotropy caused by elastic strain [16,17]. The D_{2d} point symmetry group contains the rotoreflection axis $S_4 \parallel z$, which forbids any linear polarization of emission in absence of an external magnetic field, in particular, for the no-phonon emission. Our experimental data demonstrate that the exciton emission is linearly polarized even at $B = 0$, implying the

lower C_{2v} point symmetry of the studied structure [7] being induced by nonequivalent interfaces [14]. The nonequivalent interfaces and strain induce the mixing of the heavy and light holes [18–20]which breaks equivalence of $\mathcal{X}$ and $\mathcal{Y}$ orbital Bloch functions of the valence band. As a result, the linear polarization of emission appears.

In the C_{2v} point symmetry group the components B_x and B_y of the in-plane magnetic field transform, respectively, like the vector components y and x. The combination $B_x^2 - B_y^2$ is invariant. The analysis shows that the linear polarization of emission in the (xy) set of axes can be written as [21]

$$P_l = P_0 + \mathcal{B}_1\left(B_x^2 + B_y^2\right) + \mathcal{B}_2\left(B_x^2 - B_y^2\right), \tag{1}$$

where P_0 is the intrinsic linear polarization, $\mathcal{B}_1$ and $\mathcal{B}_2$ are coefficients. Here and following in this section, we keep only contributions to the linear polarization that are quadratic in magnetic field. The parameters P_0, $\mathcal{B}_1$, and $\mathcal{B}_2$ can depend, in general, on the phonon replica, on temperature, as well as on time (under conditions of pulsed excitation) [22]. A complete description of the linear polarization of emission requires another parameter, the linear polarization in the set of axes $(x'y')$ rotated by angle $\pi/4$ with respect to the (xy) frame. The axes $(x'y')$ correspond to the cubic axes [100] and [010] in the QW plane. Accordingly, the linear polarization in the $(x'y')$ axes can be recast in the from

$$P_l' = 2\mathcal{B}' B_x B_y, \tag{2}$$

with $\mathcal{B}'$ being another independent coefficient.

Let $\varphi_{\boldsymbol{B}}$ be the angle between the magnetic field and the $x \parallel [1\bar{1}0]$ axis in the QW plane and let $\varphi/2$ be the angle between the main axis of the half-wave plate and the magnetic field. We write the polarization degree of emission detected by the half-wave plate as

$$P(\varphi_{\boldsymbol{B}}, \varphi) = P_l \cos\left(2\varphi_{\boldsymbol{B}} + 2\varphi\right) + P_l' \sin\left(2\varphi_{\boldsymbol{B}} + 2\varphi\right), \tag{3}$$

where according to Eqs. (1) and (2)

$$P_l = P_0 + \mathcal{B}_1 B^2 + \mathcal{B}_2 B^2 \cos 2\varphi_{\boldsymbol{B}}, \tag{4a}$$

$$P_l' = \mathcal{B}' B^2 \sin 2\varphi_{\boldsymbol{B}}. \tag{4b}$$

These expressions allow for direct comparison of the model and the experimental data shown in Figs. 2, 4, and 6 (see Sec. V for details).

Note that rising the symmetry up to the D_{2d} point group leads to $P_0 = 0$, $\mathcal{B}_1 = 0$ and equalizes the coefficients $\mathcal{B}_2$ and $\mathcal{B}'$. In this case, the linear polarization is solely induced by the magnetic field. The orientation of the linear polarization follows the direction of the magnetic field in the QW plane: $P(\varphi_B, 0) = \mathcal{B}_2 B^2$.

The situation becomes very rich in C_{2v} point symmetry structures [21] where, in general, all parameters P_0, $\mathcal{B}_1$, $\mathcal{B}_2$, and $\mathcal{B}'$ are independent. Our experimental data on the linear polarization orientation can indeed be accurately described by this model with a simple set of parameters: P_0 and $\mathcal{B}_1$ being nonzero and $\mathcal{B}_2 = \mathcal{B}' \equiv 0$. In this particular case,

$$P(\varphi_B, \varphi) = (P_0 + \mathcal{B}_1 B^2)\cos\left(2\varphi_{\boldsymbol{B}} + 2\varphi\right). \tag{5}$$

Indeed, the data reported in Sec. III demonstrate a nonzero value of the intrinsic linear polarization $P_0 \neq 0$, and also confirm that the magnetic field affects only the magnitude (and sign) of the linear polarization P_l in the (xy) axes frame, while linear polarization in cubic axes frame does not occur at all. Such, at first glance surprising, behavior is typical for quantum wells (see, e.g., Refs. [21,23]). The analysis performed in these works demonstrates that this situation corresponds to an "extreme" in-plane anisotropy, which results from the in-plane heavy-hole g-factor anisotropy.

In fact, in our type-II indirect band-gap GaAs/AlAs structure the electron states correspond to the $X_{x,y}$ valleys of AlAs, where the spin-orbit interaction is reduced compared to the Γ point. This makes the electron g factor practically isotropic (formally, the three principal values of the electron Landé factor tensor $g_{xx}^{(e)} \approx g_{yy}^{(e)} \approx g_{zz}^{(e)} \equiv g_e \approx 2$) [24]. By contrast, the hole states are formed in the vicinity of the Γ point of GaAs where the spin-orbit coupling is important. Moreover, in our two-monolayer thin QW interface effects are expected to be very important, and the interfaces are inherently nonequivalent [14]. The Zeeman effect for heavy holes in an in-plane magnetic field $B = (B_x, B_y, 0)$ is described by the effective Hamiltonian

$$\mathcal{H}_B^{(h)} = \frac{1}{2}\sum_{\alpha\beta} g_{\alpha\beta}\hat{\sigma}_\alpha^{(h)} B_\beta. \tag{6}$$

Here, α, β are Cartesian indices, $\hat{\sigma}_\alpha^{(h)}$ are the heavy-hole pseudospin Pauli matrices, $g_{\alpha\beta}$ are the components of the Landé factor tensor of the holes. In this work we map the hole state with angular momentum component $J_z = +\frac{3}{2}$ onto the pseudospin $j = +\frac{1}{2}$ state and vice versa in accord with Refs. [21,25,26]. The principal values of the g-factor tensor are g_{xx} and g_{yy} in the coordinate frame with $x \parallel [1\bar{1}0]$ and $y \parallel [110]$ as used here. Calculations show that the leading contributions to the parameters have the form [21,23]

$$\mathcal{B}_2, \mathcal{B}' \propto \left(\frac{\mu_B}{k_B T}\right)^2 g_e(g_{xx} + g_{yy}), \tag{7a}$$

$$\mathcal{B}_1 \propto \left(\frac{\mu_B}{k_B T}\right)^2 g_e(g_{xx} - g_{yy}). \tag{7b}$$

Here, k_B is the Boltzmann constant. We assume that $k_B T \ll \Delta_{lh-hh}$, where Δ_{lh-hh} is the splitting between the light- and heavy-hole states [9]. Since fitting of the experimental data shows that $\mathcal{B}_2$ and $\mathcal{B}'$ are equaled to zero within the experimental accuracy (see Sec. V for details), we can conclude that $g_{xx} = -g_{yy}$. Rough estimates of the parameters in the framework of the model of interface-induced or deformation-induced heavy-hole–light-hole mixing provide the following relation between the zero-field linear polarization and the anisotropic contribution to the heavy-hole g factor:

$$|g_{xx}| = |g_{yy}| = 6|\varkappa|P_0, \quad g_{xx} = -g_{yy}, \tag{8}$$

where $\varkappa$ is the magnetic Luttinger parameter [27].

B. Microscopic model

We apply the same formalism as developed in previous works [6,7], where the magnetic-field-induced circular polarization was studied.

We denote the electron states by their spin components $s = \pm\frac{1}{2}$ onto the magnetic field axis and the hole spins by their pseudospin components $j = \pm\frac{1}{2}$ along the effective field

$\sum_\beta g_{\alpha\beta}B_\beta$. In what follows, for simplicity, we assume that g_{xx} and g_{yy} have opposite signs and equal absolute values as discussed above.

The kinetic equations for the occupancies of the exciton quadruplet take the form [7]

$$\frac{df_{sj}}{dt} + \left(W^{(e)}_{\bar{s},s} + W^{(h)}_{\bar{j},j}\right)f_{sj} - W^{(h)}_{j,\bar{j}}f_{s\bar{j}} - W^{(e)}_{s,\bar{s}}f_{\bar{s}j} + \mathcal{R}f_{sj} = G_{sj}. \tag{9}$$

Here, as in previous works, $\bar{s} = -s$, $\bar{j} = -j$, the quantities G_{sj} describe the exciton generation rates, $W^{(e)}_{s,s'}$ and $W^{(h)}_{j,j'}$ are the electron and hole spin-flip rates, respectively, and the operator $\mathcal{R}$ describes the recombination of excitons. In the following, we simplify the notation for the occupation probability and replace $f_{s_z j}(s = \pm\frac{1}{2},\ j = \pm\frac{1}{2})$ by f_{ij} with $i = \pm$ and $j = \pm$, indicating the signs of s and j, respectively.

Neglecting the lateral anisotropy of the QW structure one has $\mathcal{R}f_{sj} = (1/\tau_r + 1/\tau_{nr})f_{sj}$, where τ_{nr} and τ_r are the nonradiative and radiative recombination times of excitons: Indeed, in the Voigt geometry all four exciton states have the same oscillator strengths if the heavy-hole–light-hole mixing is disregarded. In the presence of an intrinsic anisotropy, the radiative transition rates for excitons emitting light linearly polarized along the $x \parallel [1\bar{1}0]$ and $y \parallel [110]$ axes are different and the operator $\mathcal{R}$ takes the form

$$\mathcal{R}f_{++/--} = \left(\frac{1+P_0}{2\tau_r} + \frac{1}{\tau_{nr}}\right)f_{++/--}, \tag{10a}$$

$$\mathcal{R}f_{+-/-+} = \left(\frac{1-P_0}{2\tau_r} + \frac{1}{\tau_{nr}}\right)f_{+-/-+}, \tag{10b}$$

where the subscript $-+/+-$ means $-+$ *or* $+-$, and P_0 is the intrinsic degree of linear polarization. Finally, the linear polarization degree in the xy-axes frame, P_l, can be expressed in the form

$$P_l = \frac{(1+P_0)(f_{++}+f_{--}) - (1-P_0)(f_{+-}+f_{-+})}{(1+P_0)(f_{++}+f_{--}) + (1-P_0)(f_{+-}+f_{-+})}. \tag{11}$$

In Sec. V we present and analyze the full solution of the kinetic equations (9). Here, we present simplified analytical solutions which can be readily obtained for $P_0 = 0$ and for small P_0. At $P_0 = 0$ the linear polarization degree of exciton emission can be recast as

$$P_l = 4s_e s_h, \tag{12}$$

where s_e and s_h are the mean spin components of the electron and the hole,

$$s_e = \sum_{sj} s f_{sj}, \quad s_h = \sum_{sj} j f_{sj}. \tag{13}$$

Here, we have made use of the following representation for the distribution functions: $f_{++} = (1/2 + s_e)(1/2 + s_h)$, $f_{--} = (1/2 - s_e)(1/2 - s_h)$, and $f_{+-/-+} = (1/2 \pm s_e)(1/2 \mp s_h)$.

Moreover, under the experimental conditions $\tau_{nr} \gg \tau_r$, we neglect in the analytical solution the nonradiative processes completely. Thus, we obtain

$$s_i = \left(s_i^0 - \langle s_i\rangle\right)e^{-t/\tilde{\tau}_{s,i}} + \langle s_i\rangle \quad (i = e \text{ or } h). \tag{14}$$

Here, s_i^0 is the initial mean spin component of the electron or hole (it can be nonzero due to spin polarization in the course of energy relaxation toward the localized states) and $\langle s_i\rangle$ is the thermal spin polarization of the corresponding charge carrier

$$\langle s_i\rangle = -\frac{1}{2}\tanh\left(\frac{\Delta_i}{2k_BT}\right), \tag{15}$$

with $\Delta_{e,h}$ being the Zeeman splittings of the electron spin and hole pseudospin sublevels. In Eq. (14) we have introduced the effective spin relaxation times $\tilde{\tau}_{s,e}$ and $\tilde{\tau}_{s,h}$ of the charge carriers in accordance with

$$\frac{1}{\tilde{\tau}_{s,e}} = \sum_{s=\pm1/2} W^{(e)}_{s,\bar{s}}, \quad \frac{1}{\tilde{\tau}_{s,h}} = \sum_{j=\pm1/2} W^{(h)}_{j,\bar{j}}, \tag{16}$$

and we use the following definition of the transition rates:

$$W^{(i)}_{1/2,-1/2} = \frac{1}{2\tau_{s,i}}\exp\left(-\frac{\Delta_i}{k_BT}\right),$$

under the assumption of $\Delta_i > 0$. Hence, we assume that the spin-flip rates vary as functions of magnetic field only due to the exponential Boltzmann factors and neglect the weaker power-law dependence of the prefactors $\tau_{s,i}^{-1}$ on the magnetic field [28,29].

Correspondingly, the temporal dynamics of the linear polarization degree is given by

$$P_l(t) = 4\left[\left(s_e^0 - \langle s_e\rangle\right)e^{-t/\tilde{\tau}_{s,e}} + \langle s_e\rangle\right] \times \left[\left(s_h^0 - \langle s_h\rangle\right)e^{-t/\tilde{\tau}_{s,h}} + \langle s_h\rangle\right]. \tag{17}$$

In particular, if the charge carriers are initially unpolarized, $s_e^0 = s_h^0 = 0$, we have

$$P_l(t) = 4\langle s_e\rangle\langle s_h\rangle(1 - e^{-t/\tilde{\tau}_{s,e}})(1 - e^{-t/\tilde{\tau}_{s,h}}). \tag{18}$$

It follows from Eq. (18) that the linear polarization dynamics for initially unpolarized carriers is controlled by the longest relaxation time.

One can also derive an approximate expression for the polarization degree in the presence of an intrinsic linear polarization:

$$\tilde{P}_l(t) \approx \frac{P_l(t) + P_0}{1 + P_0P_l(t)}, \tag{19}$$

where $P_l(t)$ is given by Eq. (17). The product $P_0P_l(t)$ in the denominator is small as compared to unity and should be, strictly speaking, neglected. However, its inclusion provides better agreement with the full numerical calculation after Eqs. (9) and (10) for the experimentally relevant values of parameters.

In the steady state one can readily determine the polarization degree taking into account that the photoluminescence decays as $\exp(-t/2\tau_r)$. One then has

$$\begin{aligned} P_l^{st} &= \int dt\,\frac{e^{-t/2\tau_r}}{2\tau_r}P_l(t) \\ &= 4\left[\langle s_e\rangle\langle s_h\rangle + \frac{\left(s_e^0 - \langle s_e\rangle\right)\left(s_h^0 - \langle s_h\rangle\right)}{1 + \frac{2\tau_r}{\tilde{\tau}_{s,e}} + \frac{2\tau_r}{\tilde{\tau}_{s,h}}} + \frac{\left(s_e^0 - \langle s_e\rangle\right)\langle s_h\rangle}{1 + \frac{2\tau_r}{\tilde{\tau}_{s,e}}}\right. \\ &\quad \left. + \frac{\left(s_h^0 - \langle s_h\rangle\right)\langle s_e\rangle}{1 + \frac{2\tau_r}{\tilde{\tau}_{s,h}}}\right]. \end{aligned} \tag{20}$$

Typically, the first term in the brackets provides the dominant contribution since $\tau_r \gg \tilde{\tau}_{s,e}, \tilde{\tau}_{s,h}$ in the experiment. This is

typical because for long lifetimes of the excitons the steady-state value of the polarization is simply given by the equilibrium value (15). Again, taking into account the intrinsic linear polarization we approximately have

$$\tilde{P}_l^{st'} \approx \frac{P_l^{st} + P_0}{1 + P_0 P_l^{st}}. \tag{21}$$

Note that in weak magnetic fields where $|\Delta_i|/k_BT \ll 1$, the product $\langle s_e \rangle \langle s_h \rangle$ can be recast as

$$\langle s_e \rangle \langle s_h \rangle = \left(\frac{\Delta_e \Delta_h}{4k_BT} \right)^2 \propto B^2, \tag{22}$$

in agreement with the phenomenological expressions (1) and (2).

V. DISCUSSION

We start the analysis of our results by addressing the dependence of the linear polarization of exciton emission on the magnetic field strength and orientation. First, we address the data in Fig. 2, where the dependence of the intensity on the orientation of the polarizer is shown for $B = 0$. In agreement with Eqs. (3) and (4) the intensity as a function of the angle φ is given by

$$I = \frac{I_0}{2}(1 + P_0 \cos 2\varphi). \tag{23}$$

Here, I_0 is the total intensity of the emission. The resulting PL intensity as a function of the analyzer angle φ has a characteristic twofold rotational symmetry with extrema at $\varphi = 0, \pi/2, \pi$ and $3\pi/2$. For $P_0 > 0$ the intensity is maximal at $\varphi = 0$ and π and minimal at $\varphi = \pi/2$ and $3\pi/2$, in agreement with experiment.

This expression accurately fits the data shown in Fig. 2 with the value of P_0 being different for different lines. We also note that in order to reproduce the slight shift of the distribution in Fig. 2(d) an offset of about 15° should be added to φ. This offset can be related to the fact that the actual symmetry of our structure is lower than C_{2v} due to sample imperfections.

Second, we analyze the data in Fig. 4, where the magnetic field is applied in the sample plane and the three panels show the intensity distribution as a function of the magnetic field orientation with respect to the crystalline axis. In Fig. 4(a) the magnetic field angle $\varphi_{\boldsymbol{B}} = 0°$, in 4(b) 45°, and in 4(c) 90°. Accordingly, for the intensity after the polarizer we obtain

$$I = \frac{I_0}{2}[1 + (P_0 + \mathcal{B}_1 B^2 + \mathcal{B}_2 B^2)\cos 2\varphi], \tag{24a}$$

$$I = \frac{I_0}{2}[1 - (P_0 + \mathcal{B}_1 B^2)\sin 2\varphi + \mathcal{B}' B^2 \cos 2\varphi], \tag{24b}$$

$$I = \frac{I_0}{2}[1 - (P_0 + \mathcal{B}_1 B^2 - \mathcal{B}_2 B^2)\cos 2\varphi], \tag{24c}$$

for Figs. 4(a), 4(b), and 4(c), respectively. The fit of the experimental data shown in Figs. 5(e) and 5(f) after Eqs. (24) allows us to set $\mathcal{B}_2 = \mathcal{B}' = 0$ within our experimental accuracy. Thus, the magnetic field affects only the magnitude of the linear polarization for the TA_{AlAs} line, while the eigenaxes of linear polarization are fixed by the crystallographic directions $[1\bar{1}0]$ and [110].

TABLE I. Parameters of the studied ultrathin GaAs/AlAs QWs.

Parameter	Value	Comment
g_e	$+2.0$	[7]
g_{xx}	$+0.25 \pm 0.01$	Best fit
g_{yy}	-0.25 ± 0.01	Best fit
τ_r	0.34 ms	[7]
τ_{nr}	8.5 ms	[7]
τ_{sh}	3 ± 0.5 μs	[7]
τ_{se}	33 ± 1 μs	[7]
P_0	$0 \div 0.1$	Zero-field data
p_e^0	$+0.5 \pm 0.05$	Best fit
p_h^0	$+0.5 \pm 0.05$	Best fit

Third, we address the data in Fig. 6, where emission intensity at different magnetic fields is presented. For $\boldsymbol{B} \parallel [1\bar{1}0]$ we set $\varphi_{\boldsymbol{B}} = 0$ and from Eqs. (3) and (4) we obtain

$$I = \frac{I_0}{2}[1 + (P_0 + \mathcal{B}_1 + \mathcal{B}_2)B^2 \cos 2\varphi]. \tag{25}$$

The experimental data for LO_{AlAs} line can be accurately reproduced by Eq. (25) with $\mathcal{B}_2 = 0$ as well as $\mathcal{B}_1$ and P_0 having opposite signs. That is why at some particular value of magnetic field, namely, $B = 3$ T, a compensation of the intrinsic and the magnetic-field-induced contributions to the linear polarization occurs, making the intensity distribution practically isotropic. Its weak anisotropy observed in Figs. 6(c) and 6(d) can be accounted for by a slight offset of the angle φ and could be related, as already mentioned, to a symmetry lowering due to sample imperfections. Thus, the symmetry analysis of the emission intensity allows us to conclude that the studied QW structure is characterized by an extremely anisotropic hole g factor: $|\mathcal{B}_2, \mathcal{B}'| \ll |\mathcal{B}_1|$ implying $|g_{xx} - g_{yy}| \gg |g_{xx} + g_{yy}|$. As a result, we take $g_{xx} = -g_{yy}$ for our further analysis.

Let us now turn to the modeling of the magnetic-field-induced polarization and the quantitative description of the experimental data. To that end we have numerically solved the rate equations (9) after the general equation (11). We fixed the electron g factor, the radiative and nonradiative decay times of excitons, as well as the spin-flip times for electrons and holes. We take them from our previous work on magnetic-field-induced circular polarization measured for the same sample [7] (see Table I). From the fitting of the time-integrated polarization [see solid lines in Figs. 5(e) and 5(f)], we obtain the intrinsic value of the linear polarization P_0 and the heavy-hole g-factor component, $g_{xx} = -g_{yy} = 0.25$ (see Table I). We also note that for the parameters in question, the simplified analytical expression (21) with $P_l^{st} = 4\langle s_e \rangle \langle s_h \rangle$ and Eq. (15) accurately reproduces the experimental data as well.

With the very same set of parameters we perform calculations of the temporal dependence of the emission polarization shown in Fig. 7(b). The only additional ingredient of the model is the initial value of the spin polarization of the charge carriers s_i^0, which can be acquired by the electrons and holes during their energy relaxation toward the emitting states. We use expressions similar to Eq. (15):

$$s_i^0 = -\frac{1}{2}\tanh\left(\frac{p_i^0 \Delta_i}{2k_BT}\right), \tag{26}$$

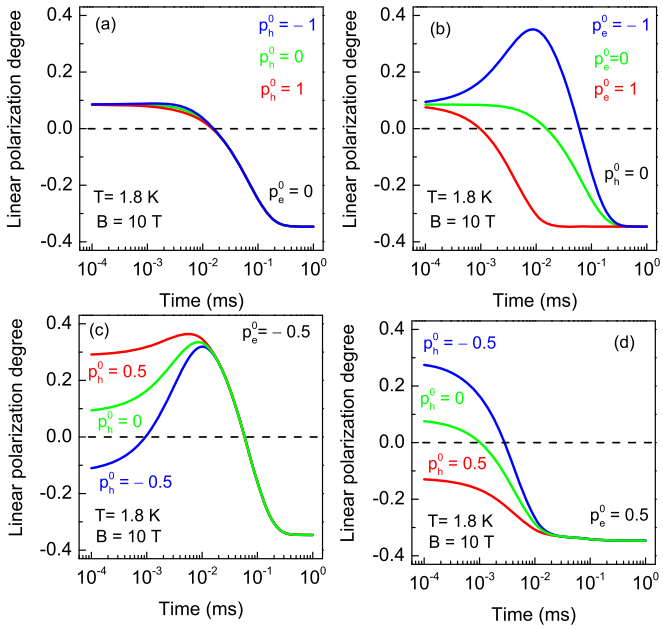

FIG. 8. Dynamics of the linear polarization degree $P_l(t)$ calculated at $B = 10$ T, $T = 1.8$ K and for the QW parameters from Table I for partial electron (p_e^0) and hole (p_h^0) spin polarization: (a) $p_e^0 = 0$ and various p_h^0, (b) $p_h^0 = 0$ and various p_e^0, (c) $p_e^0 = -0.5$ and various p_h^0, (d) $p_e^0 = 0.5$ and various p_h^0.

with the fitting parameters $-1 \leqslant p_e^0 \leqslant 1$ and $-1 \leqslant p_h^0 \leqslant 1$ to model this initial polarization. As a result, with two additional parameters p_e^0 and p_h^0 (see Table I) we can nicely describe the data in Fig. 7(b). In particular, the inclusion of $s_e^0, s_h^0 \neq 0$ allows us to reproduce the unusual temporal dynamics of the linear polarization.

In order to address the role of the initial polarization in more detail, we simulate the dynamics of the linear polarization degree. The dependencies $P_l(t)$ calculated at $B = 10$ T, $T = 1.8$ K and for the QW parameters taken from Table I for partial electron (p_e^0) and hole (p_h^0) spin polarization are shown in Fig. 8. The time during which the polarization of the emission reaches its maximum value is mainly determined by the electron spin polarization p_e^0, that was obtained in the energy relaxation process. Indeed, one can see from Fig. 8(a) that in the case of unpolarized electrons ($p_e^0 = 0$) a change in hole spin polarization does not effect the dynamics of PL polarization. On the other hand, for unpolarized holes ($p_h^0 = 0$) shown in Fig. 8(b) it is seen that a variation of the initial electron spin polarization significantly changes this dynamics. When both electrons and holes obtain partial polarization during energy relaxation, the dynamics is determined by the ratio of their polarization degrees, as shown in Figs. 8(c) and 8(d). That is why the strong dependence of the dynamics on p_e^0 and p_h^0 allows us to unambiguously determine their signs and values from fitting the experimental data shown in Fig. 7(b). The best fits are obtained for $p_e^0 = +0.5 \pm 0.05$ and $p_h^0 = +0.5 \pm 0.05$.

Thus, despite having quite a few model parameters, our analysis allows us to fix most of them from independent analyses and describe accurately the experimental data. The resulting values are quite realistic. Indeed, as discussed in Sec. IV A and Ref. [23] the intrinsic linear polarization can be related with an anisotropic contribution to the heavy-hole in-plane g factor under the assumption that both effects result from the heavy-hole–light-hole mixing. It follows from Eq. (8) that for $P_0 \sim 5\% \ldots 10\%$ and the magnetic Luttinger parameter $|\varkappa|$ ranging from 0.12 (AlAs) to 1.2 (GaAs) [30] we obtain absolute values of $g_{xx} = -g_{yy}$ in the range from 0.004 to 0.72 with the experimental value of 0.25 being within this range. Additionally, the anisotropic contribution to the heavy-hole Landé factor can arise from in-plane localization of the excitons.

VI. CONCLUSIONS

We have investigated experimentally and theoretically the magneto-optical properties of a two-monolayer-thick GaAs/AlAs quantum well, which is indirect both in real and in momentum space, as function of magnetic field strength and orientation.

We have found the following features of the linear polarization degree of the QW exciton photoluminescence: (i) Already at zero field nonzero linear polarization appears. Its absolute value has a strong spectral dependence across the emission band of the QW being about 3.5% for the no-phonon (NP) line, zero for the (TA) phonon-assisted recombination line, 9.5% and 6% for the (LO) and (2LO) phonon-assisted recombination lines, respectively. (ii) The effect of the magnetic field applied in the Voigt geometry on the orientation of the linear polarization with respect to the crystallographic axes of the QW and its degree is determined only by the field strength for all observed PL lines at a fixed temperature and does not depend on the field orientation in the QW plane. (iii) Unexpectedly, the linear polarization degree demonstrates a long-lasting temporal dynamics in magnetic field.

A very good quantitative description of all experimental data is obtained using a model with just a few variable parameters, which can be unambiguously determined from the data. The developed approach can readily be used for investigation of the spin dynamics in semiconductor quantum well and quantum dot structures with indirect band gap either in real or in momentum space, or in both of them.

ACKNOWLEDGMENTS

The authors are grateful to E.L. Ivchenko for discussions. This work was supported by the Deutsche Forschungsgemeinschaft Project No. 409810106, the Russian Foundation for Basic Research Grant No. 19-52-12001, and by the Act 211 Government of the Russian Federation (Contract No. 02.A03.21.0006). Government of the Russian Federation also supports this work via Grant No. AAAA-A17-117042110141-5. On the German side, also the support in the frame of the ICRC TRR 160 by the Deutsche Forschungsgemeinschaft is acknowledged. The Russian Foundation for Basic Research also supported T.S.S. via Grant No. 19-02-00098. M.M.G. is grateful to Saint-Petersburg State University for the research Grant No. 11.34.2.2012 (ID No. 28874264) and the Russian Foundation for Basic Research Project No. 19-52-12038.

[1] *Optics of Semiconductors and Their Nanostructures*, edited by H. Kalt and M. Hetterich (Springer, Berlin, 2004).

[2] C. F. Klingshirn, *Semiconductor Optics* (Springer, Heidelberg, 2012).

[3] G. Wang, A. Chernikov, M. M. Glazov, T. F. Heinz, X. Marie, T. Amand, and B. Urbaszek, Colloquium: Excitons in atomically thin transition metal dichalcogenides, Rev. Mod. Phys. **90**, 021001 (2018).

[4] T. Karin, X. Linpeng, M. M. Glazov, M. V. Durnev, E. L. Ivchenko, S. Harvey, A. K. Rai, A. Ludwig, A. D. Wieck, and K.-M. C. Fu, Giant permanent dipole moment of two-dimensional excitons bound to a single stacking fault, Phys. Rev. B **94**, 041201(R) (2016).

[5] D. S. Smirnov, K. G. Belyaev, D. A. Kirilenko, M. O. Nestoklon, M. V. Rakhlin, A. A. Toropov, I. V. Sedova, S. V. Sorokin, S. V. Ivanov, B. Gil, and T. V. Shubina, Exciton bound to 1D intersection of stacking fault plane with a ZnSe quantum well, Phys. Status Solidi (RRL) **12**, 1700410 (2018).

[6] T. S. Shamirzaev, J. Debus, D. R. Yakovlev, M. M. Glazov, E. L. Ivchenko, and M. Bayer, Dynamics of exciton recombination in strong magnetic fields in ultrathin GaAs/AlAs quantum wells with indirect band gap and type-II band alignment, Phys. Rev. B **94**, 045411 (2016).

[7] T. S. Shamirzaev, J. Rautert, D. R. Yakovlev, J. Debus, A. Yu. Gornov, M. M. Glazov, E. L. Ivchenko, and M. Bayer, Spin dynamics and magnetic field induced polarization of excitons in ultrathin GaAs/AlAs quantum wells with indirect band gap and type-II band alignment, Phys. Rev. B **96**, 035302 (2017).

[8] G. Danan, B. Etienne, F. Mollot, R. Planel, A. M. Jean-Louis, F. Alexandre, B. Jusserand, G. Le Roux, J. Y. Marzin, H. Savary and B. Sermage, Optical evidence of the direct-to-indirect-gap transition in GaAs-A1As short-period superlattices, Phys. Rev. B **35**, 6207 (1987).

[9] T. S. Shamirzaev, A. M. Gilinsky, A. K. Kalagin, A. V. Nenashev, and K. S. Zhuravlev, Energy spectrum and structure of thin pseudomorphic InAs quantum wells in an AlAs matrix: Photoluminescence spectra and band-structure calculations, Phys. Rev. B **76**, 155309 (2007).

[10] We chose for this study a very thin GaAs QW in order to be able to compare its properties to another InAs/AlAs model QW structure, which has an indirect band gap, but a type-I band alignment. Due to strain, high-quality InAs/AlAs QWs can be grown with a few monolayer thickness only. This does not represent a crucial limitation for a GaAs/AlAs heterostructure, for which QWs can be grown with wider widths.

[11] L. P. Fu, F. T. Bacalzo, G. D. Gilliland, R. Chen, K. K. Baja, J. Klem, and D. J. Wolford, Microscopic mechanisms governing exciton-decay kinetics in type-II GaAs/AlAs supperlattices, Phys. Rev. B **52**, 2682 (1995).

[12] W. A. J. A. van der Poel, A. L. G. J. Severens, H. W. van Kesteren, and C. T. Foxon, Spin relaxation in type-II GaAs/AlAs quantum wells, Phys. Rev. B **39**, 8552 (1989).

[13] *Physics of Group IV Elements and III-V Compounds*, edited by O. Madelung, M. Schulz, and H. Weiss, Landolt-Börnstein Numerical Data and Relationships, New Series, Group III (Springer, Berlin, 1982), Vol. 17, Pt. a.

[14] D. S. Abramkin, A. K. Gutakovskii, and T. S. Shamirzaev, Heterostructures with diffused interfaces: Luminescent technique for ascertainment of band alignment type, J. Appl. Phys. **123**, 115701 (2018).

[15] T. Belhadj, T. Amand, A. Kunold, C.-M. Simon, T. Kuroda, M. Abbarchi, T. Mano, K. Sakoda, S. Kunz, X. Marie, and B. Urbaszek, Impact of heavy hole-light hole coupling on optical selection rules in GaAs quantum dots, Appl. Phys. Lett. **97**, 051111 (2010).

[16] E. L. Ivchenko, *Optical Spectroscopy of Semiconductor Nanostructures* (Alpha Science, Harrow UK, 2005).

[17] M. M. Glazov, *Electron & Nuclear Spin Dynamics in Semiconductor Nanostructures* (Oxford University Press Oxford, 2018).

[18] I. L. Aleiner and E. L. Ivchenko, Anistropic exchange splitting in type II GaAs/AlAs superlattices, Pis'ma Zh. Eksp. Teor. Fiz. **55**, 662 (1992) [JETP Lett. **55**, 692 (1992)].

[19] G. E. Pikus and F. G. Pikus, The mechanism of heavy and light hole mixing in GaAs/AlAs superlattices, Solid State Commun. **89**, 319 (1994).

[20] E. L. Ivchenko, A. Yu. Kaminski, and U. Roessler, Heavy-light hole mixing at zinc-blende (001) interfaces under normal incidence, Phys. Rev. B **54**, 5852 (1996).

[21] Yu. G. Kusrayev, A. V. Koudinov, I. G. Aksyanov, B. P. Zakharchenya, T. Wojtowicz, G. Karczewski, and J. Kossut, Extreme In-Plane Anisotropy of the Heavy-Hole g Factor in (001)- CdTe/CdMnTe Quantum Wells, Phys. Rev. Lett. **82**, 3176 (1999).

[22] With allowance for the higher-order in B effects these parameters can depend on the magnetic field strength as well.

[23] A. V. Koudinov, N. S. Averkiev, Yu. G. Kusrayev, B. R. Namozov, B. P. Zakharchenya, D. Wolverson, J. J. Davies, T. Wojtowicz, G. Karczewski, and J. Kossut, Linear polarization of the photoluminescence of quantum wells subject to in-plane magnetic fields, Phys. Rev. B **74**, 195338 (2006).

[24] J. Debus, T. S. Shamirzaev, D. Dunker, V. F. Sapega, E. L. Ivchenko, D. R. Yakovlev, A. I. Toropov, and M. Bayer, Spin-flip Raman scattering of the Γ-X mixed exciton in indirect band gap (In,Al)As/AlAs quantum dots, Phys. Rev. B **90**, 125431 (2014).

[25] In some cases, it is convenient to use another mapping where $J_z = \pm\frac{3}{2}$ corresponds to $j = \mp\frac{1}{2}$, in which case $g_{xx} \to g_{xx}$ and $g_{yy} \to -g_{yy}$ [17].

[26] X. Marie, T. Amand, P. Le Jeune, M. Paillard, P. Renucci, L. E. Golub, V. D. Dymnikov, and E. L. Ivchenko, Hole spin quantum beats in quantum-well structures, Phys. Rev. B **60**, 5811 (1999).

[27] E. L. Ivchenko and G. E. Pikus, *Superlattices and Other Heterostructures* (Springer, Berlin, 1997).

[28] L. M. Woods, T. L. Reinecke, and Y. Lyanda-Geller, Spin relaxation in quantum dots, Phys. Rev. B **66**, 161318(R) (2002).

[29] X. Linpeng, T. Karin, M. V. Durnev, R. Barbour, M. M. Glazov, E. Ya. Sherman, S. P. Watkins, S. Seto, and K.-M. C. Fu, Longitudinal spin relaxation of donor-bound electrons in direct band-gap semiconductors, Phys. Rev. B **94**, 125401 (2016).

[30] I. Vurgaftman, J. R. Meyer, and L. R. Ram-Mohan, Band parameters for III-V compound semiconductors and their alloys, J. Appl. Phys. **89**, 5815 (2001).